Ion Optics of Sector-Type Magnetic Focusing Fields

AUTHOR(S):

KADOTA, Noriaki; ISHIDA, Seiichi

CITATION:

KADOTA, Noriaki ...[et al]. Ion Optics of Sector-Type Magnetic Focusing Fields. Memoirs of the Faculty of Engineering, Kyoto University 1960, 22(1): 41-67

ISSUE DATE:

1960-03-10

URL:

http://hdl.handle.net/2433/280459

Ion Optics of Sector-Type Magnetic Focusing Fields

By

Noriaki KADOTA* and Seiichi ISHIDA*

(Received October 31, 1959)

The convergence of the ion beam in the sector-type magnetic focusing field of the mass spectrometer is treated geometrically. The real thickness of the ion beam was considered, and the ratio of the radius of deflection to the beam thickness is included as a common parameter in the expression for the final image width. The treatment is composed of three parts: the first order approximation, the second order approximation and the complete convergence. In conclusion, a new type of optical system consisting of a dual arrangement of circular magnetic fields, is proposed and given the name "Collimatron" optical system.

1. Introduction

A variety of treatments has been reported in detail on the mass dispersion and refocusing of charged particles in the electromagnetic field by Henneberg[1], Herzog[2], Mattauch[3], Hintenberger[4], Kerwin[5] et al., but some important problems still remain untreated. From the standpoint of the theory of geometrical ion optics, the magnetic boundary proposed by Kerwin is essentially an ideal one which assumes that there is no fringing effect at the boundary of the magnet and that all the ion beams are emitted from a point source. But it is inevitable that in the actual instrument problems such the fringing field effect, the existence of thickness in the ion beam, the space charge effect etc. are encountered. Even if they are suitably corrected, it is not easy to obtain the Kerwin-field boundary in actual instruments. We must, therefore, adopt approximations for the field boundaries in actual instruments. It is soon evident from a geometrical analysis that a Kerwin-field would not provide perfect focusing for an ion beam with real thickness, and much less could be expected of the approximations to it. It would seem important, therefore, to get information on the convergence of an ion beam with thickness and divergence. On introducing these two parameters, it is found convenient to treat them in terms of the ratio of the deflection radius of the beam to its thickness, which is defined as the "thickness coefficient, n". The amount of aberration is expressed as the total image width, which means the image of

* Department of Fuel Chemistry.

the source slit on the collector plate corresponding to the thickness and divergence of the ion beam. The treatments are confined to the π-, $\pi/2$- and $\pi/3$-type magnetic fields, for they are usually adopted in practice. First, the convergence of a beam with divergence but no thickness and that of a beam with both divergence and thickness are compared in the first order approximation. For the second order approximation, though the fundamental treatment of Hintenberger and the instrumentation of Davies[6] have been reported, the treatment is devised to get the radius of curvature of the magnet boundary for a beam of definite divergence. The authors adopted their image width method in the second as well as in the first order approximation, though the numerical computations become more complicated. The radius of curvature of the magnetic boundaries is given as a definite value, which is readily introduced as the radius of curvature at the intersection of the central incident beam with Kerwin's ideal boundary. In all these treatments, the fringing field effect is cancelled out by means of Nier's approximation[7], though that approximation may be unsuitable for such a precise treatment as the present one. Finally, from the fact that the Kerwin-field can be theoretically divided into two fields, which can be replaced by the second order approximation in the $\pi/2$- field, the authors propose a new type of magnetic focusing field, in which spherical aberration does not exist for an ion beam with both thickness and wide divergence. Compound magnetic fields of this type are called "Collimatron" configurations by the authors.

2. Nomenclature of Symbols

When an ion beam with thickness and divergence is treated, the image width must be discussed with reference to each beam group, which may lead to complexity in description. Therefore, the symbols are defined as follows and all descriptions are made symbolically.

O : Ion beam leaving the most outside edge (from the center of deflection) of the ion source slit.

O': Arrival point of beam O on the collector plate.

C : Ion beam leaving the center of the ion source slit.

C': Arrival point of beam C on the collector plate.

I : Ion beam leaving the most inside edge of the ion source slit.

I' : Arrival point of beam I on the collector plate.

Moreover, the following suffixes are added to these symbols to indicate the divergence angle and thickness of the ion beam.

$O(^{0}_{\cdots})$, $C(^{0}_{\cdots})$, $I(^{0}_{\cdots})$, $O(^{\pm\theta}_{\cdots})$, $C(^{\pm\theta}_{\cdots})$, $I(^{\pm\theta}_{\cdots})$: The central beam is indicated by the symbol $(^{0}_{\cdots})$, the ion beam divergent by θ outside the central beam by $(^{+\theta}_{\cdots})$,

and the ion beam divergent by θ inside the central beam by $(\overset{-\theta}{\cdots})$.
$O(\overset{0}{n})$, $I(\overset{0}{n})$, $O(\overset{\pm\theta}{n})$, $I(\overset{\pm\theta}{n})$: n is called the "thickness coefficient" and the thickness of the ion beam is expressed by $2r/n$ (r is the radius of deflection), e.g. beam C is composed of $C(\overset{+\theta}{\infty})$, $C(\overset{0}{\infty})$ and $C(\overset{-\theta}{\infty})$. With the use of these symbols, $O'(\overset{+\theta}{n})$ indicates the image position of the ion beam leaving the most outside edge of the source slit with thickness coefficient n and diverging by θ outside, on the collector plate.

Next symbols and suffixes are used with regard to the image on the collector plate.

S: Distance between the collector plate center and the image position on the collector plate (image width).

$S_{\pi \text{ or } \pi/2 \text{ or } \pi/3}(\overset{\cdots}{\cdots})$ indicates that the deflection angle of the ion beam is π, or $\pi/2$ or $\pi/3$.

$S^{O \text{ or } I \text{ or } C}(\overset{\cdots}{\cdots})$ indicates the image width of $O(\overset{\cdots}{\cdots})$, or $C(\overset{\cdots}{\cdots})$ or $I(\overset{\cdots}{\cdots})$.

Example: $S^{I}_{\pi/2}(\overset{\cdots}{\cdots})$ indicates the image width of $I(\overset{\cdots}{\cdots})$ beam in $\pi/2$-type deflection field.

$\mathfrak{S}$: Total (or Maximum) image width, taking all S's into account.

Thus, if S^{+} and S^{-} are image widths outside and inside the collector plate center, $\mathfrak{S}$ is given as follows,

$$\mathfrak{S} = S^{+}_{\max} + |S^{-}_{\max}| .$$

3. Focusing in the Magnetic Field with the Linear Boundary[8)]

3.1. Focusing in the $\pi/2$-type Magnetic Field

3.1.1. Ion Beam with Divergence but No Thickness

Fig. 1 clearly shows that of the ion beams with thickness perpendicular to the center line on the paper surface, the beams $C(\overset{+\theta}{\infty})$ and $C(\overset{-\theta}{\infty})$, divergent by $\pm\theta$ from the central beam $C(\overset{0}{\infty})$ and entering perperdicularly the magnetic field, do not converge at the central point of the ion collector plate and, therefore, produce the well-known image width.

The estimation of this image width can be made by means of analytical geometry. Using the co-ordinate system of Fig. 1, the beam with divergence angle $+\theta$ is expressed by the equation,

$$y = x \cdot \tan\theta + r(2 + \tan\theta) , \tag{1}$$

and has its center of curvature, M_{c+} (x_{cc}, y_{cc}), at the point, i.e.,

$$x_{cc} = r \cdot \sin\theta , \quad y_{cc} = r(2 + \tan\theta - \cos\theta) . \tag{2}$$

And now the image width is found from the following formula, taking $C(\overset{-\theta}{\infty})$ into account,

$$S^{C}_{\pi/2}(\overset{\pm\theta}{\infty}) = r\left[\sin\theta - \frac{1-(1-t)(2-t)}{\sqrt{(2-t)\cdot t}} - 1\right], \tag{3}$$

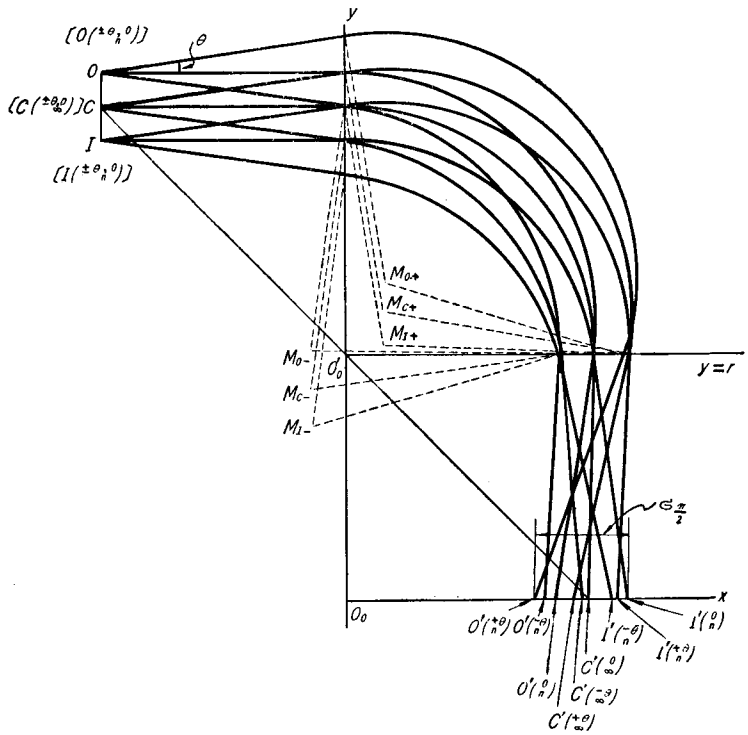

Fig. 1. Image width in $\pi/2$-type focusing field with linear boundary.

where $t=\cos\theta-\tan\theta$. A negative or positive value of the image width indicates, as seen from the figure, that the image lies inside or outside of $C'(^{0}_{\infty})$. Fig. 4 shows the relation of the image width to the divergence angle, from which it is found that both $C'(^{+\theta}_{\infty})$ and $C'(^{-\theta}_{\infty})$ lie inside $C'(^{0}_{\infty})$; and further, that

$$|S^{C}_{\pi/2}(^{+\theta}_{\infty})|>|S^{C}_{\pi/2}(^{-\theta}_{\infty})|\,, \tag{4}$$

so that the estimation of the image width is made possible by calculating $|S^{C}_{\pi/2}(^{+\theta}_{\infty})|$ only. The total image width, therefore, is written as follows,

$$\mathfrak{S}^{C}_{\pi/2}(^{\pm\theta}_{\infty}) = |S^{C}_{\pi/2}(^{+\theta}_{\infty})|\,. \tag{5}$$

3. 1. 2. Ion Beam with both Thickness and Divergence

In the preceding section, the problem was dealt with on the assumption that the ion beam has divergence only and no thickness, corresponding to $n=\infty$ as the limit of the thickness. Practically, however, even if other aberrations might be negligibly small, it is necessary to give the beam a width at least as large as the final slit width of the ion source, which requires us to consider the image width, taking the beam thickness into account.

This raises the problem as to how to introduce the thickness into the equation for the image width. It is convenient to use the thickness coefficient, n. In the mass spectrometer actually used, $n=500\sim5{,}000$, which corresponds to $0.007\sim0.7$ mm as the final slit width of the ion source for the usual dimensions of the instrument. Almost all the estimations were made for this range of the value of n.

For the calculation, the beams to be taken into account are divided into three groups, making nine beams in total, i.e., $O(^{+\theta}_{n})$, $O(^{0}_{n})$, $O(^{-\theta}_{n})$; $C(^{+\theta}_{\infty})$, $C(^{0}_{\infty})$, $C(^{-\theta}_{\infty})$; $I(^{+\theta}_{n})$, $I(^{0}_{n})$, $I(^{-\theta}_{n})$, but the three beams in the middle group may be omitted, for they have been treated previously.

3. 1. 2a. Focusing of $O(^{\pm\theta,\,0}_{n})$

This beam group is represented by the equation,

$$y = x\cdot\tan\theta + r\left(2+\frac{1}{n}+\tan\theta\right), \tag{6}$$

and the center of curvature of $O(^{+\theta}_{n})$, $M_{0+}(x_{0c}, y_{0c})$, is found as follows,

$$x_{0c} = r\cdot\sin\theta, \quad y_{0c} = r\left(2+\frac{1}{n}+\tan\theta-\cos\theta\right). \tag{7}$$

The image width, using the same symbols as in the case of the ion beam with no thickness, is expressed by the following equation,

$$S^{0}_{\pi/2}(^{\pm\theta,\,0}_{n}) = r\left[\sin\theta+\frac{1-\left(2-t+\frac{1}{n}\right)\left(1-t+\frac{1}{n}\right)}{\sqrt{\left(2-t+\frac{1}{n}\right)\left(t-\frac{1}{n}\right)}}-1\right]. \tag{8}$$

As seen from above, all images lie inside $C'(^{0}_{\infty})$, and,

$$S^{0}_{\pi/2}(^{0}_{n}) = r\left[\frac{1-\frac{1}{n}-\frac{1}{n^2}}{\sqrt{1-\frac{1}{n^2}}}-1\right]. \tag{9}$$

Comparison of the three image positions shows that $O(^{+\theta}_{n})$ has its image most inside $C'(^{0}_{\infty})$, and the total image width is written in the form,

$$\mathfrak{S}^{0}_{\pi/2}(^{\pm\theta,\,0}_{n}) = |S^{0}_{\pi/2}(^{+\theta}_{n})|. \tag{10}$$

3. 1. 2b. Focusing of $I(^{\pm\theta,\,0}_{n})$

The following equation expresses this beam group.

$$y = x\cdot\tan\theta + r\left(2-\frac{1}{n}+\tan\theta\right). \tag{11}$$

And the center of curvature of $I(^{+\theta}_{n})$, $M_{I+}(x_{Ic}, y_{Ic})$, is expressed by the equation,

$$x_{Ic} = r\cdot\sin\theta, \quad y_{Ic} = r\left(2-\frac{1}{n}+\tan\theta-\cos\theta\right). \tag{12}$$

Then the image width of this group is given as follows.

$$S^{I}_{\pi/2}(^{\pm\theta,\,0}_{n}) = r\left[\sin\theta + \frac{1-\left(2-t-\frac{1}{n}\right)\left(1-t-\frac{1}{n}\right)}{\sqrt{\left(2-t-\frac{1}{n}\right)\left(t+\frac{1}{n}\right)}} - 1\right]. \tag{13}$$

where $t=\cos\theta-\tan\theta$. In this case, all three images lie outside of $C'(^{0}_{\infty})$, in contrast to the preceding case. Further, as known from eq. (13),

$$S^{I}_{\pi/2}(^{0}_{n}) = r\left[\frac{1+\frac{1}{n}-\frac{1}{n^2}}{\sqrt{1-\frac{1}{n^2}}} - 1\right], \tag{14}$$

so that, if an ion beam group consists of three beam i.e., $O(^{0}_{n})$, $C(^{0}_{\infty})$ and $I(^{0}_{n})$, all of which are focused at one point as they leave the plane of the magnetic field, after when $O(^{0}_{n})$ and $I(^{0}_{n})$ diverge from $C(^{0}_{\infty})$ and the total image width due to them is represented by the formula,

$$\mathfrak{S}^{0,\,I}_{\pi/2}(^{0}_{n}) = \frac{2}{\sqrt{1-\frac{1}{n^2}}}\frac{r}{n}, \tag{15}$$

i.e., $1/\sqrt{1-1/n^2}$ times the thickness of the ion beam. Moreover, because

$$|S^{0}_{\pi/2}(^{0}_{n})| > S^{I}_{\pi/2}(^{0}_{n}) \tag{16}$$

when the beam has a considerable thickness, $O'(^{0}_{n})$ lies farther from $C'(^{0}_{\infty})$ than $I'(^{0}_{n})$, but the positions of these two images are symmetrical with regard to $C'(^{0}_{\infty})$, when $n>500$, which is the actual case. From a comparison of these three beams we find that $I(^{0}_{n})$ focuses most outside of $C'(^{0}_{\infty})$ on the collector plate when the divergence angle is small, and that the total image width of the beam with both thickness and divergence in the $\pi/2$ magnetic field is written in the following form,

$$\mathfrak{S}_{\pi/2}(^{\pm\theta,\,0}_{n,\,\infty}) = |S^{0}_{\pi/2}(^{+\theta}_{n})| + S^{I}_{\pi/2}(^{0}_{n}). \tag{17}$$

These results, along with those for the case of $n=\infty$ as reference, are tabulated in Table 1, in which the positive and negative signs are referred to $S^{I}_{\pi/2}(^{0}_{n})$ and $S^{0}_{\pi/2}(^{+\theta}_{n})$, respectively, and the total image width is obtained by adding their absolute values.

3. 2. Focusing in the $\pi/3$-type Magnetic Field

3. 2. 1. Ion Beam with Divergence but No Thickness

The co-ordinate system is chosen as shown in Fig. 2, and the derivation proceeds in the same way as in the $\pi/2$-field. The ion beam divergent by $+\theta$ from the central beam is expressed by the equation,

$$y = x\cdot\tan\theta + r(2+\sqrt{3}\tan\theta), \tag{18}$$

and has the center of curvature, $M_{c+}(x_{cc}, y_{cc})$, at the point, i.e.,

$$x_{cc} = r\cdot\sin\theta, \quad y_{cc} = r(2+\sqrt{3}\tan\theta-\cos\theta). \tag{19}$$

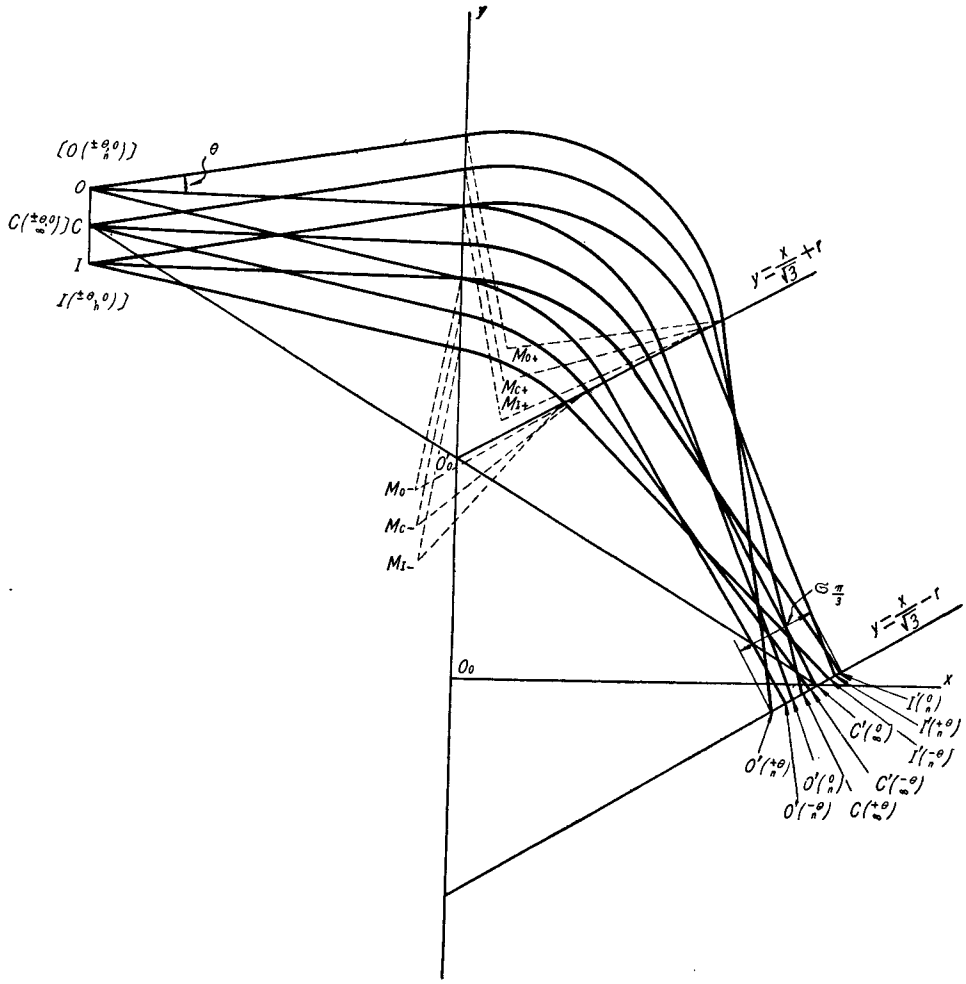

Fig. 2. Image width in $\pi/3$-type focusing field with linear boundary.

This beam, leaving the magnetic boundary expressed by the equation $y=(1/\sqrt{3})x+r$ at the point $B_{c+}(x_{bc}, y_{bc})$, has its image $C'(^{+\theta}_{\infty})$ on the collector plate reproduced by the equation $y=(1/\sqrt{3})x-r$. x_{bc} and y_{bc} are given as below,

$$\begin{aligned} x_{bc} &= \frac{\sqrt{3}}{4}\left\{\sqrt{3}\,x_{cc}-r+y_{cc}+\sqrt{r^2+6ry_{cc}-3y_{cc}^2-2\sqrt{3}\,x_{cc}(r-y_{cc})-x_{cc}^2}\right\} \\ y_{bc} &= \frac{1}{4}\left\{\sqrt{3}\,x_{cc}+3r+y_{cc}+\sqrt{r^2+6ry_{cc}-3y_{cc}^2-2\sqrt{3}\,x_{cc}(r-y_{cc})-x_{cc}^2}\right\}, \end{aligned} \tag{20}$$

and the co-ordinate (x, y) of $C'(^{+\theta}_{\infty})$ is given by the following form,

$$\begin{aligned} x &= \sqrt{3}\left\{\frac{r^2+(r+y_{cc})(y_{bc}-y_{cc})+x_{cc}(x_{bc}-x_{cc})}{\sqrt{3}\,(x_{bc}-x_{cc})+(y_{bc}-y_{cc})}\right\} \\ y &= \frac{r^2(r+y_{cc})(y_{bc}-y_{cc})+x_{cc}(x_{bc}-x_{cc})}{\sqrt{3}\,(x_{bc}-x_{cc})+(y_{bc}-y_{cc})}\,. \end{aligned} \tag{21}$$

While $\overline{C'(^{+\theta}_{\infty})C'(^{0}_{\infty})}=2y$, the substitution of (x_{cc}, y_{cc}) and (x_{bc}, y_{bc}) into y in eq. (21), taking $C(^{-\theta}_{\infty})$ into account, gives the image width as follows,

$$S^{C}_{\pi/3}(^{\pm\theta}_{\infty}) = \frac{r}{2}\left[\frac{4-(\varphi+\sqrt{3})^2-2\sqrt{3}(\varphi+\sqrt{3})}{\sqrt{1-\varphi^2-2\sqrt{3}\,\varphi}} + \sqrt{3}\tan\theta-2\sin\left(\frac{\pi}{6}-\theta\right)-1\right], \tag{22}$$

where $\varphi=3\tan\theta-2\sin(\pi/3+\theta)$. The equation is plotted in Fig. 4 along with that of the $\pi/2$-field. These two beams $C(^{\pm\theta}_{\infty})$ both focus inside of $C'(^{0}_{\infty})$, and then,

$$|S^{C}_{\pi/3}(^{+\theta}_{\infty})|>|S^{C}_{\pi/3}(^{-\theta}_{\infty})|\,. \tag{23}$$

The total image width, as in the $\pi/2$-field, can be estimated by considering $|S^{C}_{\pi/3}(^{+\theta}_{\infty})|$ only and expressed by the following equation,

$$\mathfrak{S}^{C}_{\pi/3}(^{\pm\theta}_{\infty}) = |S^{C}_{\pi/3}(^{+\theta}_{\infty})|\,. \tag{24}$$

3. 2. 2. Ion Beam with both Thickness and Divergence

As in the $\pi/2$ magnetic field, the two beam groups $O(^{\pm\theta,\,0}_{n})$ and $I(^{\pm\theta,\,0}_{n})$ are treated separately in the calculation of their image widths.

3. 2. 2a. Focusing of $O(^{\pm\theta,\,0}_{n})$

For example, the $O(^{+\theta}_{n})$ beam is expressed by the equation,

$$y = x\cdot\tan\theta+r\left(2+\frac{1}{n}+\sqrt{3}\tan\theta\right), \tag{25}$$

and its center of curvature $M_{0+}(x_{0c}, y_{0c})$, is found to have the following coordinates,

$$x_{0c} = r\cdot\sin\theta\,,\quad y_{0c} = r\left(2+\frac{1}{n}+\sqrt{3}\tan\theta-\cos\theta\right). \tag{26}$$

Proceeding as before with the same symbols yields the following equation for the image width,

$$S^{0}_{\pi/3}(^{\pm\theta,\,0}_{n}) = \frac{r}{2}\left[\frac{4-\left\{\varphi+\sqrt{3}\left(1+\frac{1}{n}\right)\right\}^2-2\sqrt{3}\left\{\varphi+\sqrt{3}\left(1+\frac{1}{n}\right)\right\}}{\sqrt{1-\varphi^2-2\sqrt{3}\,\varphi-\frac{2\sqrt{3}}{n}\varphi-\frac{3}{n^2}(2n+1)}} + \sqrt{3}\tan\theta-2\sin\left(\frac{\pi}{6}-\theta\right)-\left(1-\frac{1}{n}\right)\right]. \tag{27}$$

Furthermore, the relation between the sign of the image width value eq. (27) and the image position is the same as described above, and therefore, all images are found inside of $C'(^{0}_{\infty})$. Moreover, it is clear from the image formula that

$$|S^{0}_{\pi/3}(^{+\theta}_{n})|>|S^{0}_{\pi/3}(^{-\theta}_{n})|\,. \tag{28}$$

Therefore, $O(^{+\theta}_{n})$ focuses most inside of $C'(^{0}_{\infty})$, and the total image width can be written in the following form,

$$\mathfrak{S}^{0}_{\pi/3}(^{\pm\theta,\,0}_{n}) = |S^{0}_{\pi/3}(^{+\theta}_{n})| \,. \tag{29}$$

3. 2. 2b. Focusing of $I(^{\pm\theta,\,0}_{n})$

This beam group is represented by the equation,

$$y = x\cdot\tan\theta + r\left(2-\frac{1}{n}+\sqrt{3}\,\tan\theta\right), \tag{30}$$

and the center of curvature of $I(^{+\theta}_{n})$, $M_{I+}(x_{Ic},\, y_{Ic})$, is given in the form,

$$x_{Ic} = r\cdot\sin\theta\,, \quad y_{Ic} = r\left(2-\frac{1}{n}+\sqrt{3}\,\tan\theta-\cos\theta\right). \tag{31}$$

And then, the image width for this group is written as follows,

$$S^{I}_{\pi/3}(^{\pm\theta,\,0}_{n}) = \frac{r}{2}\left[\frac{4-\left\{\varphi+\sqrt{3}\left(1-\frac{1}{n}\right)\right\}^{2}-2\sqrt{3}\left\{\varphi+\sqrt{3}\left(1-\frac{1}{n}\right)\right\}}{\sqrt{1-\varphi^{2}-2\sqrt{3}\,\varphi+\frac{2\sqrt{3}}{n}\varphi-\frac{3}{n^{2}}(2n+1)}}\right.$$

$$\left.+\sqrt{3}\,\tan\theta-2\sin\left(\frac{\pi}{6}-\theta\right)-\left(1+\frac{1}{n}\right)\right], \tag{32}$$

where φ is the same as before. In this case, the beam group has its image outside of $C'(^{0}_{\infty})$, just as in the case of the $\pi/2$-field. And then, it is clear from the formula (32), that

$$S^{0}_{\pi/3}(^{0}_{n}) < 0\,, \quad S^{I}_{\pi/3}(^{0}_{n}) > 0\,. \tag{33}$$

Therefore, the beam group consisting of the three beams $O(^{0}_{n})$, $C(^{0}_{\infty})$ and $I(^{0}_{n})$, is focused on the line $y=r$, and then $O(^{0}_{n})$ and $I(^{0}_{n})$ diverge from $C(^{0}_{\infty})$, giving the following image width,

$$\mathfrak{S}^{0I}_{\pi/3}(^{0}_{n}) = r\left[\frac{6}{\sqrt{(2n+1)(2n-1)}}-\frac{1}{n}\right]. \tag{34}$$

Further, when the beam has considerable thickness,

$$|S^{0}_{\pi/3}(^{0}_{n})| < S^{I}_{\pi/3}(^{0}_{n})\,, \tag{35}$$

but, if n is larger than 500, these two images lie symmetrically with respect to $C'(^{0}_{\infty})$. Consequently, as in the $\pi/2$-field, the total image width is reproduced by the following formula,

$$\mathfrak{S}_{\pi/3}(^{\pm\theta,\,0}_{n,\,\infty}) = |S^{0}_{\pi/3}(^{+\theta}_{n})| + S^{I}_{\pi/3}(^{0}_{n})\,. \tag{36}$$

These results are given in Table 2.

Table 1. Positions of both ends of total image in $\pi/2$ linear boundary field. (in r unit)

n \ θ	1°	2°	3°	4°
100	−0.0105 0.1000	−0.0117 0.1000	−0.0136 0.1000	−0.0163 0.1000
500	−0.0024 0.0020	−0.0033 0.0020	−0.0051 0.0020	−0.0076 0.0020
1,000	−0.0013 0.0010	−0.0023 0.0010	−0.0040 0.0010	−0.0065 0.0010
2,000	−0.0009 0.0005	−0.0017 0.0005	−0.0035 0.0005	−0.0060 0.0005
5,000	−0.0005 0.0002	−0.0015 0.0002	−0.0032 0.0002	−0.0056 0.0002
∞	−0.0005	−0.0014	−0.0031	−0.0053

Table 2. Positions of both ends of total image in $\pi/3$ linear boundary field. (in r unit)

n \ θ	1°	2°	3°	4°
100	−0.0106 0.1000	−0.0118 0.1000	−0.0140 0.1000	−0.0164 0.1000
500	−0.0025 0.0020	−0.0034 0.0020	−0.0053 0.0020	−0.0078 0.0020
1,000	−0.0015 0.0010	−0.0024 0.0010	−0.0041 0.0010	−0.0067 0.0010
2,000	−0.0010 0.0005	−0.0018 0.0005	−0.0037 0.0005	−0.0062 0.0005
5,000	−0.0006 0.0002	−0.0016 0.0002	−0.0033 0.0002	−0.0058 0.0002
∞	−0.0005	−0.0014	−0.0032	−0.0056

3. 3. Focusing in π-type Magnetic Field

3. 3. 1. Ion Beam with Divergence but No Thickness

As is clear from Fig. 3, the two beams $C(^{+\theta}_{\infty})$ and $C(^{-\theta}_{\infty})$ focus inside $C'(^{0}_{\infty})$ at one point $(2r\cdot\cos\theta,\ 0)$, while $C(^{0}_{\infty})$ focuses at the point $(2r,\ 0)$, and, therefore, the image width is written as follows,

$$\mathfrak{S}^{c}_{\pi}(^{\pm\theta}_{\infty}) = |S^{c}_{\pi}(^{\pm\theta}_{\infty})| = |2r\,(\cos\theta - 1)|\,. \tag{37}$$

These results are shown in Fig. 4 along with those for the $\pi/2$- and $\pi/3$-fields.

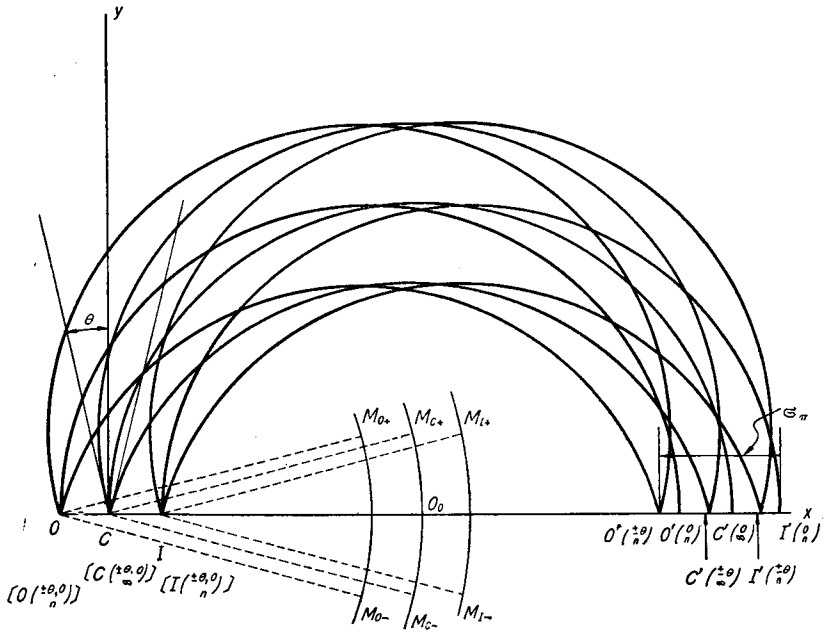

Fig. 3. Image width in π-type focusing field with linear boundary.

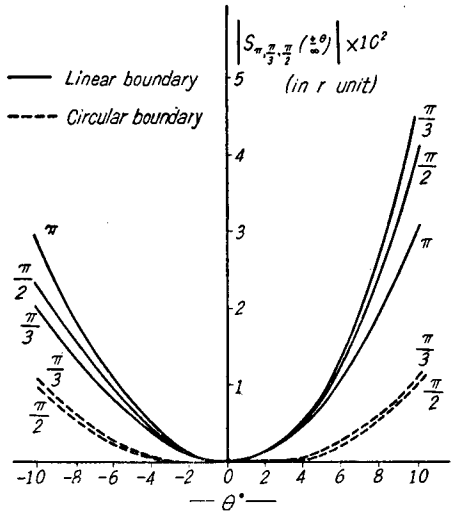

Fig. 4. The relation of image width to divergence angle in both linear and circular boundary fields.

3. 3. 2. Ion Beam with both Thickness and Divergence

Fig. 3 shows that $O(\frac{+\theta}{n})$ focuses most inside of $C'(\frac{0}{\infty})$ and $I(\frac{0}{n})$ most outside, as in the other two cases.

3. 3. 2a. Focusing of $O(^{\pm\theta,\,0}_{n})$

In contrast to the $\pi/2$- and $\pi/3$-fields, the two beams $O(^{+\theta}_{n})$ and $O(^{-\theta}_{n})$ focus at one point $(2r\cdot\cos\theta - r/n, 0)$, and the $O(^{0}_{n})$ at the point $(2r-r/n, 0)$. The image width is represented by the formula,

$$\mathfrak{S}^{0}_{\pi}(^{\pm\theta,\,0}_{n}) = -\left[2r(1-\cos\theta)+\frac{r}{n}\right]. \tag{38}$$

3. 3. 2b. Focusing of $I(^{\pm\theta,\,0}_{n})$

Also in this case, the two beams $I(^{+\theta}_{n})$ and $I(^{-\theta}_{n})$ have their images at the same point $(2r\cdot\cos\theta + r/n, 0)$, and $I(^{0}_{n})$ at the point $(2r+r/n, 0)$. Therefore, the two parallel beams $O(^{0}_{n})$ and $I(^{0}_{n})$ after crossing and then diverging, focus symmetrically on the two sides of $C'(^{0}_{\infty})$; and in the π-field, the image width due to the two parallel beams is actually written as follows,

$$\mathfrak{S}^{0I}_{\pi}(^{0}_{n}) = \frac{2r}{n}\ \text{(thickness of beam)}. \tag{39}$$

Generally, the image width of $I(^{\pm\theta,\,0}_{n})$ is expressed by the equation,

$$\mathfrak{S}^{I}_{\pi}(^{\pm\theta,\,0}_{n}) = -\left[2r(1-\cos\theta)-\frac{r}{n}\right]. \tag{40}$$

Finally, the total image width is written in the following form,

$$\mathfrak{S}_{\pi}(^{\pm\theta,\,0}_{n,\,\infty}) = 2r(1-\cos\theta)+\frac{2r}{n}. \tag{41}$$

This equation shows that the total image width increases just by the thickness of the beam, which is quite different from the situations in the other fields.

4. Focusing in the Magnetic Field with Circular Boundary

4. 1. Circular Approximation to the Kerwin Field

The Kerwin field with no spherical aberration gives the ideal magnetic boundary for an ion beam with no actual thickness, but with divergence. With this field applied to $\pi/2$- and $\pi/3$-fields (Figs. 5 and 6), the magnetic boundaries are reproduced by the following two equations (42) and (43),

$$y = \frac{x(\sqrt{2}\,r-x)}{\sqrt{r^2-x^2}} \tag{42}$$

and

$$y = \frac{x(2r-x)}{\sqrt{r^2-x^2}}, \tag{43}$$

where r is the radius of deflection.

Therefore, if the pole pieces can be shaped according the above derived functional curves corresponding to the deflection angles, a so-called bright mass spectrometer will be obtained. But, it is technically difficult to shape the pole pieces exactly in agreement with such complex curves as these; and even if

shaping should be possible, it is extremely difficult to set accurately the analyser tube relative to the magnetic field. Therefore, the Kerwin field itself is only of theoretical importance. The circular approximation may be established by

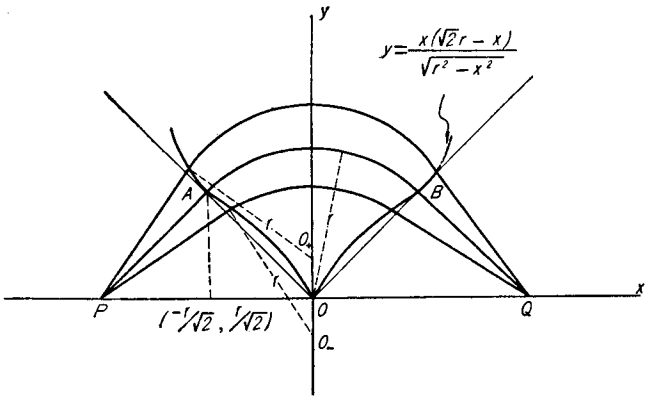

Fig. 5. $\pi/2$-type Kerwin field.

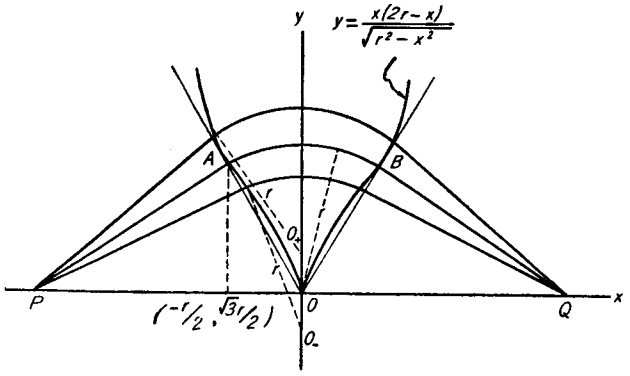

Fig. 6. $\pi/3$-type Kerwin field.

estimating the radius of curvature of the Kerwin field at the incident points of the central beams to the field, and shaping the incident and exit boundaries of the field with these approximate radii.

Generally, the radius of curvature, ρ, at any point on the curve $f(x)$ is obtained by the equation,

$$\rho = \frac{\{1+(dy/dx)^2\}^{3/2}}{d^2y/dx^2} .$$

In the case of the $\pi/2$-type spectrometer, the incident point of the central beam has the co-ordinates $(-r/\sqrt{2}, r/\sqrt{2})$ from eq. (42), and in the case of the $\pi/3$-type, $(-r/2, \sqrt{3}\, r/2)$, from eq. (43), so the following results are obtained.

$$\rho_{\pi/2} = r \quad \text{and} \quad \rho_{\pi/3} = 3\sqrt{3} \cdot r .$$

Consequently, the radius of the circular boundary to be used is r or $3\sqrt{3} \cdot r$ according to whether the deflection angle is $\pi/2$ or $\pi/3$.

4. 2. Focusing in the $\pi/2$-type Magnetic Field

4. 2. 1. Ion Beam with Divergence but No Thickness

The center of the deflection field, M, is taken as the origin of the co-ordinate system as shown in Fig. 7, and the ion beam $C(^{+\theta}_{\infty})$ divergent by $+\theta$ from the central beam $C(^{0}_{\infty})$ is expressed by the equation,

$$y = x \cdot \tan\theta + 2r \cdot \tan\theta , \tag{44}$$

and the incident point $A_{c+}(x_{ac}, y_{ac})$ is the intersection of the straight line

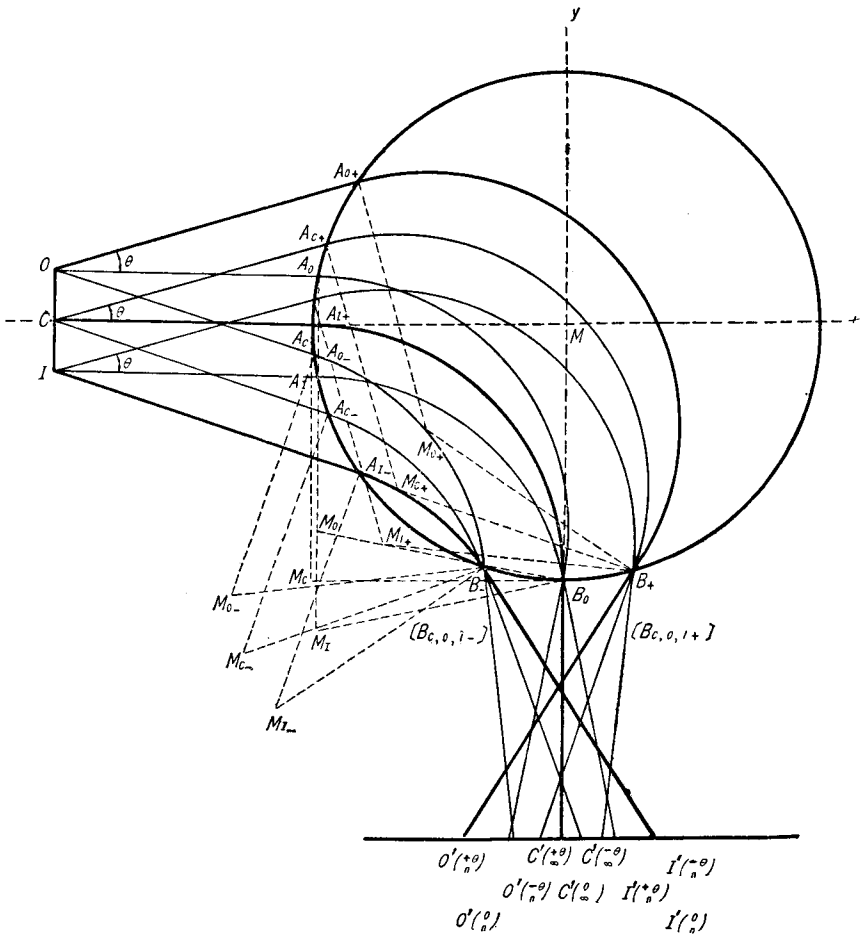

Fig. 7. Image width in $\pi/2$-type focusing field with circular boundary.

expressed by eq. (44) with the circular boundary, expressed by the equation,

$$x^2+y^2=r^2, \tag{45}$$

with the following co-ordinates.

$$\begin{aligned} x_{ac} &= -r\left\{2\sin^2\theta+\cos\theta\sqrt{\alpha\beta}\right\} \\ y_{ac} &= r\left\{2\sin\theta\cos\theta-\sin\theta\sqrt{\alpha\beta}\right\}. \\ \alpha &= 1+2\sin\theta, \quad \beta = 1-2\sin\theta. \end{aligned} \tag{46}$$

Then, the deflection center of this beam, $M_c+(x_{cc}, y_{cc})$, is found as follows,

$$\begin{aligned} x_{cc} &= x_{ac}+r\cdot\sin\theta \\ y_{cc} &= y_{ac}-r\cdot\cos\theta. \end{aligned} \tag{47}$$

From eqs. (46) and (47) the following result is obtained,

$$\begin{aligned} x_{cc} &= r\left\{\sin\theta(1-2\sin\theta)-\cos\theta\sqrt{\alpha\beta}\right\}, \\ y_{cc} &= -r\left\{\cos\theta(1-2\sin\theta)+\sin\theta\sqrt{\alpha\beta}\right\}, \end{aligned} \tag{48}$$

and the point of departure from the magnetic field, $B_c+(x_{bc}, y_{bc})$, is the intersection of the circular boundary expressed by eq. (45) with the circle with radius r and center at (x_{cc}, y_{cc}), the general expression (49) for the co-ordinates being,

$$\begin{aligned} x_{bc} &= \frac{1}{2}\left\{x_{cc}-y_{cc}\sqrt{\frac{4r^2}{x_{cc}^2+y_{cc}^2}-1}\right\}, \\ y_{bc} &= \frac{1}{2}\left\{y_{cc}+x_{cc}\sqrt{\frac{4r^2}{x_{cc}^2+y_{cc}^2}-1}\right\}. \end{aligned} \tag{49}$$

The substitution of eq. (48) and eq. (49) gives the following simple result.

$$\begin{aligned} x_{bc} &= r\cdot\sin\theta \\ y_{bc} &= -r\cdot\cos\theta. \end{aligned} \tag{50}$$

Finally, the intersection of this beam with the collector plate expressed by $y=-2r$, which is directly obtained as the intersection of the tangential line of the circle and the straight line, gives the image width as the x-co-ordinate as follows,

$$S^C_{\pi/2}(^{\pm\theta}_{\infty}) = -2r\cdot\sin\theta\left\{\frac{2\cos\theta-\sqrt{\alpha\beta}-1}{2\sin^2\theta+\cos\theta\sqrt{\alpha\beta}}\right\}. \tag{51}$$

The sign in this formula is positive or negative according to whether the image lies outside or inside $C'(^{0}_{\infty})$. As is clear from the formula, $C'(^{+\theta}_{\infty})$ lies inside of $C'(^{0}_{\infty})$ and $C'(^{-\theta}_{\infty})$ outside. Therefore,

$$|S^C_{\pi/2}(^{+\theta}_{\infty})| = S^C_{\pi/2}(^{-\theta}_{\infty}), \tag{52}$$

so that, the image positions of these beams are symmetrical to $C'(\overset{0}{\infty})$, from which the total image width is in this case obtained from the following expression,

$$\mathfrak{S}^{C}_{\pi/2}(\overset{\pm\theta}{\infty}) = 2|S^{C}_{\pi/2}(\overset{+\theta}{\infty})|\,, \tag{53}$$

i.e., by doubling the image width due to $C(\overset{+\theta}{\infty})$ (or $C(\overset{-\theta}{\infty})$).

The total image width of the ion beam with divergence but no thickness in the $\pi/2$-type mass spectrometer is evaluated and plotted in Fig. 4 in relation to the divergence angle, which shows that the image width becomes more narrow and sharper with the circular boundary than with the linear boundary, and much more so when the divergence angle is large.

4. 2. 2. Ion Beam with both Thickness and Divergence

As before, the total beam is divided into three, $O(\overset{\pm\theta;\,0}{n})$, $C(\overset{\pm\theta;\,0}{\infty})$ and $I(\overset{\pm\theta;\,0}{n})$ and the evaluation of the image width will be made with the two beam groups $O(\overset{\pm\theta;\,0}{n})$ and $I(\overset{\pm\theta;\,0}{n})$, because $C(\overset{\pm\theta;\,0}{\infty})$ gives a smaller image width than the others and has already been discussed.

4. 2. 2a. Focusing of $O(\overset{\pm\theta;\,0}{n})$

This beam group is expressed in the equation,

$$y = x\cdot\tan\theta + r\left(2\tan\theta + \frac{1}{n}\right), \tag{54}$$

and the incident point of this beam into the magnetic field $A_{0+}(x_{a0},\ y_{a0})$, is given below,

$$\begin{aligned} x_{a0} &= -r\left\{2\sin^2\theta + \frac{\sin\theta\cos\theta}{n} + \cos\theta\sqrt{\alpha'\beta'}\right\} \\ y_{a0} &= \quad r\left\{2\sin\theta\cos\theta + \frac{\cos^2\theta}{n} - \sin\theta\sqrt{\alpha'\beta'}\right\}. \\ \alpha' &= 1+2\sin\theta+\frac{\cos\theta}{n}, \quad \beta' = 1-2\sin\theta-\frac{\cos\theta}{n}. \end{aligned} \tag{55}$$

The deflection center, $M_{0+}(x_{c0},\ y_{c0})$ is given as follows,

$$\begin{aligned} x_{c0} &= \quad r\left\{\beta'\sin\theta - \cos\theta\sqrt{\alpha'\beta'}\right\} \\ y_{c0} &= -r\left\{\beta'\cos\theta + \sin\theta\sqrt{\alpha'\beta'}\right\}. \end{aligned} \tag{56}$$

Then the determination of the point of departure from the field gives the same point as with $C(\overset{\pm\theta}{\infty})$, i.e., $x_{b0}=x_{bc}$, $y_{b0}=y_{bc}$, and finally the image width is estimated to be as follows.

$$\begin{aligned} S^{0}_{\pi/2}(\overset{\pm\theta;\,0}{n}) = {} & \frac{-r}{2\sin^2\theta + \frac{\sin\theta\cos\theta}{n} + \cos\theta\sqrt{\alpha'\beta'}} \times \\ & \left\{4\sin\theta\cos\theta - 2\sin\theta - 2\sin\theta\sqrt{\alpha'\beta'} + \frac{\cos\theta}{n}(2\cos\theta - 1)\right\}. \end{aligned} \tag{57}$$

In this case, both images lie inside of $C'(^{0}_{\infty})$, and then,

$$|S^{0}_{\pi/2}(^{+\theta}_{n})|>|S^{0}_{\pi/2}(^{-\theta}_{n})|\,. \tag{58}$$

Moreover, $O(^{0}_{n})$ has the following image width,

$$S^{0}_{\pi/2}(^{0}_{n}) = -\frac{r}{n}\left(\frac{1}{\sqrt{1-\frac{1}{n^2}}}\right), \tag{59}$$

focusing inside $C'(^{0}_{\infty})$ as well as $O(^{\pm\theta}_{n})$, but the next relation holds in this case,

$$|S^{0}_{\pi/2}(^{+\theta}_{n})|>|S^{0}_{\pi/2}(^{0}_{n})|\,, \tag{60}$$

and consequently the total image width is written in the form,

$$\mathfrak{S}^{0}_{\pi/2}(^{\pm\theta,\,0}_{n}) = |S^{0}_{\pi/2}(^{+\theta}_{n})|\,. \tag{61}$$

4. 2. 2b. Focusing of $I(^{\pm\theta,\,0}_{n})$

The $I(^{+\theta}_{n})$ beam group is expressed by the following equation,

$$y = x\cdot\tan\theta + r\left(2\tan\theta-\frac{1}{n}\right), \tag{62}$$

and the evaluation of the incident point into the magnetic field, $A_{I+}(x_{aI},\ y_{aI})$, and the center of deflection, $M_{I+}(x_{cI},\ y_{cI})$ gives the following results,

$$\begin{aligned} x_{aI} &= -r\left\{2\sin^2\theta-\frac{\sin\theta\cos\theta}{n}+\cos\theta\sqrt{\alpha''\beta''}\right\} \\ y_{aI} &= \quad r\left\{2\sin\theta\cos\theta-\frac{\cos^2\theta}{n}-\sin\theta\sqrt{\alpha''\beta''}\right\} \\ \alpha'' &= 1+2\sin\theta-\frac{\cos\theta}{n},\quad \beta'' = 1-2\sin\theta+\frac{\cos\theta}{n}, \end{aligned} \tag{63}$$

and

$$\begin{aligned} x_{cI} &= \quad r\left\{\sin\theta-\cos\theta\sqrt{\alpha''\beta''}\right\} \\ y_{cI} &= -r\left\{\cos\theta+\sin\theta\sqrt{\alpha''\beta''}\right\}. \end{aligned} \tag{64}$$

And the points of departure from the field have the same co-ordinates as $O(^{\pm\theta}_{n})$, $(r\cdot\sin\theta,\ -r\cdot\cos\theta)$. Thus, in the $\pi/2$-type mass spectrometer with a circular magnetic boundary, ion beam groups divergent by θ outside or by θ inside leave the field at the point B_+ $(r\cdot\sin\theta,\ -r\cdot\cos\theta)$ or B_- $(-r\cdot\sin\theta,\ -r\cdot\cos\theta)$, respectively, regardless of their thickness.

Finally, the image position on the collector plate is given by the formula,

$$\begin{aligned} S^{I}_{\pi/2}(^{\pm\theta,\,0}_{n}) = {} & \frac{-r}{2\sin^2\theta-\frac{\sin\theta\cos\theta}{n}+\cos\theta\sqrt{\alpha''\beta''}}\times \\ & \left\{4\sin\theta\cos\theta-2\sin\theta-2\sin\theta\sqrt{\alpha''\beta''}-\frac{\cos\theta}{n}(2\cos\theta-1)\right\}. \end{aligned} \tag{65}$$

Now both images lie outside $C'(^{0}_{\infty})$, having the following relation,

$$S^I_{\pi/2}(^{-\theta}_{n}) > S^I_{\pi/2}(^{+\theta}_{n}) \tag{66}$$

and as for $I(^{0}_{n})$,

$$S^I_{\pi/2}(^{0}_{n}) = \frac{r}{n}\frac{1}{\sqrt{1-\frac{1}{n^2}}}\left[= -S^0_{\pi/2}(^{0}_{n})\right] \tag{67}$$

and

$$S^I_{\pi/2}(^{-\theta}_{n}) > S^I_{\pi/2}(^{0}_{n}) \tag{68}$$

are obtained.

Summarising the above, the beams focusing most outside and most inside are $I(^{-\theta}_{n})$ and $O(^{+\theta}_{n})$, respectively, and these two image positions are, as known from above equations, symmetrical with regard to $C'(^{0}_{\infty})$, i.e., the following relation is obtained,

$$S^I_{\pi/2}(^{-\theta}_{n}) = |S^0_{\pi/2}(^{+\theta}_{n})| . \tag{69}$$

The total image width, therefore, is represented by the formula,

$$\mathfrak{S}_{\pi/2}(^{\pm\theta,\,0}_{n,\,\infty}) = 2|S^0_{\pi/2}(^{+\theta}_{n})| = 2S^I_{\pi/2}(^{-\theta}_{n}) , \tag{70}$$

and the evaluation of either the $O(^{+\theta}_{n})$ or $I(^{-\theta}_{n})$ beam enables us to calculate the total image width, for which the results are shown in Table 3. The sign, positive or negative, has the same meaning as in the linear boundary field, though the distinction of the sign of the image width is not necessary in the present case due to the symmetry of the image with regard to the original point on the collector plate.

4.3. Focusing in the $\pi/3$-type Magnetic Field

4.3.1. Ion Beam with Divergence but No Thickness

The same treatment as in the $\pi/2$-field is possible, and the center of curvature of the incident plane to the magnetic field is different from that of the plane at departure from the field, which makes the calculation troublesome if the origin of the co-ordinate system is not suitably chosen. So, at first, the origin is put at the center of curvature, O_1, of the incident plane (Fig. 8) and then moved to the center of curvature, O_2, of the leaving plane, which simplifies the numerical calculation of the image width.

The incident beam, when the origin is set at O_1, is expressed by the equation,

$$y = x\cdot\tan\theta + 4_V\sqrt{3}\cdot r\cdot\tan\theta . \tag{71}$$

While the incident boundary is expressed by the circular equation,

$$x^2+y^2 = (3_V\sqrt{3}\cdot r)^2 , \tag{72}$$

so that the incident point $A_{c+}(x_{ac}, y_{ac})$ and the center of deflection $M_{c+}(x_{cc}, y_{cc})$ are given by the following two sets of equations,

$$
\begin{aligned}
x_{ac} &= -r\left\{4\sqrt{3}\sin^2\theta + \sqrt{3}\cos\theta\sqrt{\gamma\delta}\right\}, \\
y_{ac} &= r\left\{4\sqrt{3}\sin\theta\cos\theta - \sqrt{3}\sin\theta\sqrt{\gamma\delta}\right\}, \\
\gamma &= 3+4\sin\theta, \quad \delta = 3-4\sin\theta,
\end{aligned}
\tag{73}
$$

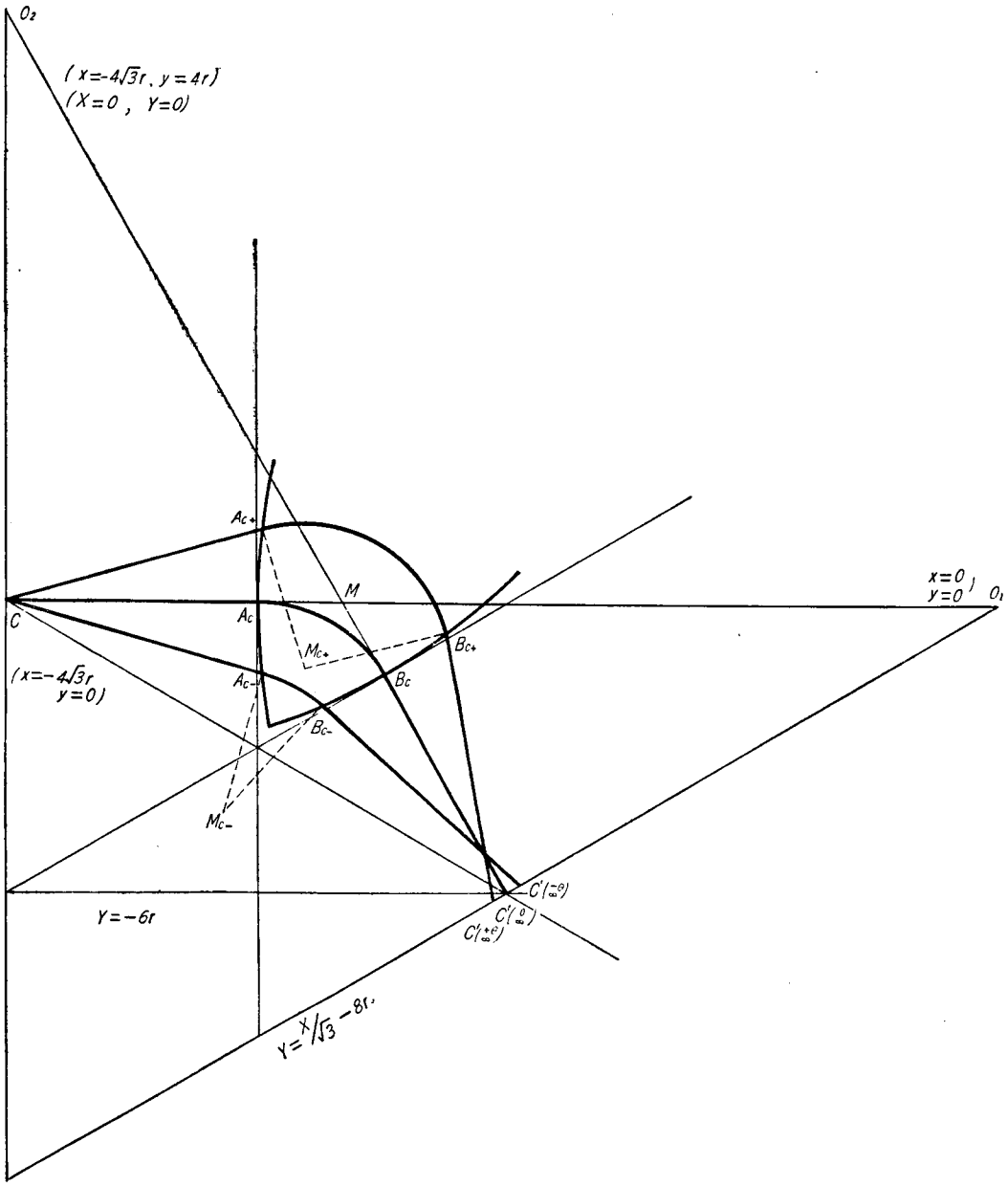

Fig. 8. Focusing in $\pi/3$-type field with circular boundary (only central beam group described).

and,

$$\left.\begin{aligned} x_{cc} &= r\left\{\sin\theta(1-4\sqrt{3}\sin\theta)-\sqrt{3}\cos\theta\sqrt{7\delta}\right\}, \\ y_{cc} &= -r\left\{\cos\theta(1-4\sqrt{3}\sin\theta)+\sqrt{3}\sin\theta\sqrt{7\delta}\right\}. \end{aligned}\right\} \tag{74}$$

Now the origin is moved to the center of curvature of the leaving plane, and the new co-ordinate of the deflection center becomes (X_{cc}, Y_{cc}), so that the next relation must hold between the present and the former co-ordinates of the point.

$$\left.\begin{aligned} X_{cc} &= x_{cc}+4\sqrt{3}\,r \\ Y_{cc} &= y_{cc}-4r. \end{aligned}\right\} \tag{75}$$

Therefore, the points of departure $B_{c+}(X_{bc}, Y_{bc})$ in the new co-ordinate is given by the following equations,

$$\left.\begin{aligned} X_{bc} &= \frac{u+13r^2}{2u}\left\{X_{cc}-Y_{cc}\sqrt{\frac{54ur^2}{(u+13r^2)^2}-1}\right\} \\ Y_{bc} &= \frac{u+13r^2}{2u}\left\{Y_{cc}+X_{cc}\sqrt{\frac{54ur^2}{(u+13r^2)^2}-1}\right\}. \end{aligned}\right\} \tag{76}$$

$$u = (X_{cc}^2+Y_{cc}^2)/2$$

As discussed before, any further expression for the image width becomes too complicated, so the evaluation was made only numerically after equation (76) was obtained. Then the intersection of the beam with the collector plate, i.e., the straight line expressed by the equation $Y=(X/\sqrt{3})-8r$, is given below,

$$Y = \frac{r^2+(8r+Y_{cc})(Y_{bc}-Y_{cc})+X_{cc}(X_{bc}-X_{cc})}{\sqrt{3}\,(X_{bc}-X_{cc})+(Y_{bc}-Y_{cc})}-8r, \tag{77}$$

but, the image width to be required in practice is the length measured along the collector plate, and so, from the figure, it may be written as follows,

$$S^C_{\pi/3}(^{\pm\theta}_{\infty}) = 2(Y+6). \tag{78}$$

As in the $\pi/2$-type field, the image positions in this case are symmetrical with respect to $C'(^{0}_{\infty})$ and the negative or positive sign has the same meaning as in the $\pi/2$-type case.

Consequently, the total image width is given by the following expression,

$$\mathfrak{S}^C_{\pi/3}(^{\pm\theta}_{\infty}) = 2\left|S^C_{\pi/3}(^{+\theta}_{\infty})\right|. \tag{79}$$

This result is illustrated in Fig. 4 together with that for the $\pi/2$-type mass spectrometer, which shows that the image width is clearly more narrow than in the case of a linear boundary field.

4. 3. 2. Ion Beam with both Thickness and Divergence

This treatment must also proceed by dividing the ion beams into $O(^{\pm\theta,\,0}_{n})$,

$C(^{\pm\theta;}_{\infty\ 0})$ and $I(^{\pm\theta;}_{n\ 0})$, and the calculation was performed numerically as in the previous section, because of the complicated character of the formal expressions. So the results of the calculation will be shown here. The co-ordinate system in this case is chosen in the same way as in the preceding system, i.e., at first the origin is put at O_1, and then moved to O_2. The points of entrance into the magnetic field:

As for $O(^{\pm\theta;}_{n\ 0})$,

$$\begin{aligned} x_{a0} &= -r\left\{4\sqrt{3}\sin^2\theta+\frac{\sin\theta\cos\theta}{n}+\sqrt{3}\cos\theta\sqrt{\gamma'\delta'}\right\} \\ y_{a0} &= r\left\{4\sqrt{3}\sin\theta\cos\theta+\frac{\cos^2\theta}{n}-\sqrt{3}\sin\theta\sqrt{\gamma'\delta'}\right\}. \end{aligned} \tag{80}$$

$$\gamma' = 3+4\sin\theta+\frac{\cos\theta}{\sqrt{3}\,n},\quad \delta' = 3-4\sin\theta-\frac{\cos\theta}{\sqrt{3}\,n}$$

As for $I(^{\pm\theta;}_{n\ 0})$,

$$\begin{aligned} x_{aI} &= -r\left\{4\sqrt{3}\sin^2\theta-\frac{\sin\theta\cos\theta}{n}+\sqrt{3}\cos\theta\sqrt{\gamma''\delta''}\right\} \\ y_{aI} &= r\left\{4\sqrt{3}\sin\theta\cos\theta-\frac{\cos^2\theta}{n}-\sqrt{3}\sin\theta\sqrt{\gamma''\delta''}\right\}. \end{aligned} \tag{81}$$

$$\gamma'' = 3+4\sin\theta-\frac{\cos\theta}{\sqrt{3}\,n},\quad \delta'' = 3-4\sin\theta+\frac{\cos\theta}{\sqrt{3}\,n}$$

The centers of deflection:

As for $O(^{\pm\theta;}_{n\ 0})$,

$$\begin{aligned} x_{c0} &= r\left\{\sin\theta(1-4\sqrt{3}\sin\theta)-\frac{\sin\theta\cos\theta}{n}-\sqrt{3}\cos\theta\sqrt{\gamma'\delta'}\right\} \\ y_{c0} &= -r\left\{\cos\theta(1-4\sqrt{3}\sin\theta)-\frac{\cos^2\theta}{n}+\sqrt{3}\sin\theta\sqrt{\gamma'\delta'}\right\}. \end{aligned} \tag{82}$$

As for $I(^{\pm\theta;}_{n\ 0})$,

$$\begin{aligned} x_{cI} &= r\left\{\sin\theta(1-4\sqrt{3}\sin\theta)+\frac{\sin\theta\cos\theta}{n}-\sqrt{3}\cos\theta\sqrt{\gamma''\delta''}\right\} \\ y_{cI} &= -r\left\{\cos\theta(1-4\sqrt{3}\sin\theta)+\frac{\cos^2\theta}{n}+\sqrt{3}\sin\theta\sqrt{\gamma''\delta''}\right\}. \end{aligned} \tag{83}$$

After these points are obtained, the origin is moved to the center of curvature, O_2, the points of departure obtained, and then the image width estimated with the use of the intersection of the beams with the collector plate, which is omitted. However, the result is, as in the $\pi/2$-type case, that the image of $O(^{+\theta}_{n})$ lies most inside, the image of $I(^{-\theta}_{n})$ most outside, and the two images are symmetrical with respect to $C'(^{0}_{\infty})$. The total image width is given in the form,

$$\mathfrak{S}_{\pi/3}(^{\pm\theta;}_{n,\infty\ 0}) = 2|S^0_{\pi/3}(^{+\theta}_{n})| = 2S^I_{\pi/3}(^{-\theta}_{n}), \tag{84}$$

and the results of the calculation are shown in Table 4. Tables 1~4 show that the circular approximation for the magnetic boundary is remarkably superior to the linear approximation for the convergence of a beam with wide divergence,

Table 3. Positions of both ends of total image in $\pi/2$ circular boundary field. (in r unit)

n \ θ	1°	2°	3°	4°
100	−0.0101 0.0101	−0.0101 0.0101	−0.0104 0.0104	−0.0108 0.0108
500	−0.0020 0.0020	−0.0021 0.0021	−0.0023 0.0023	−0.0027 0.0027
1,000	−0.0010 0.0010	−0.0011 0.0011	−0.0012 0.0012	−0.0019 0.0019
2,000	−0.0006 0.0006	−0.0006 0.0006	−0.0008 0.0008	−0.0012 0.0012
5,000	−0.0003 0.0003	−0.0003 0.0003	−0.0005 0.0005	−0.0009 0.0009
∞	0 0	−0.0001 0.0001	−0.0003 0.0003	−0.0007 0.0007

Table 4. Positions of both ends of total image in $\pi/3$ circular boundary field. (in r unit)

n \ θ	1°	2°	3°	4°
100	−0.0101 0.0101	−0.0102 0.0102	−0.0105 0.0105	−0.0110 0.0110
500	−0.0020 0.0020	−0.0021 0.0021	−0.0024 0.0024	−0.0028 0.0028
1,000	−0.0010 0.0010	−0.0011 0.0011	−0.0013 0.0013	−0.0020 0.0020
2,000	−0.0006 0.0006	−0.0006 0.0006	−0.0009 0.0009	−0.0013 0.0013
5,000	−0.0003 0.0003	−0.0003 0.0003	−0.0006 0.0006	−0.0010 0.0010
∞	0 0	−0.0001 0.0001	−0.0003 0.0003	−0.0008 0.0008

but though it is less so for beams with large thickness. It may, therefore, be concluded that, in the case of the circular approximation, improvement in the resolving power should not be expected when the final slit of the ion source has a wide opening. This is an important result for the designing of a mass spectrometer, especially for the precise electromagnetic mass separator.

4.4. Test Pole Pieces in Second-Order Approximation with Nier Correction for the Fringing Field Effect

The test pole pieces for a $\pi/2$-type field of the second order approximation

were made as shown in Fig. 9. They were shaped out of a forged mild steel block especially offered as the magnet material by the Sumitomo Kinzoku Co. As in the linear boundary field, the fringing effect was considered in this case and correction for that effect was included in the design of the pieces, by applying Nier's approximation. Nier's approximation was at first an empirical method for

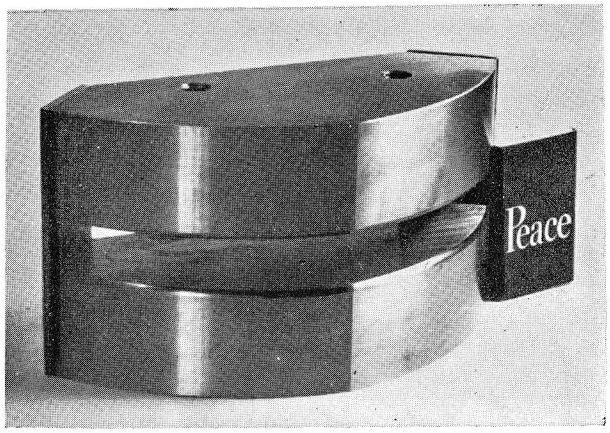

Fig. 9. Pole pieces that the second-order approximation for focusing and Nier's approximation for fringing correction are applied to, with deflection angle of $\pi/2$.

correcting the fringing effect, but is supported theoretically by Coggeshall[9], though recently Sugawara[10] showed that this method of approximation has a slight deviation. The authors, however, adopted this approximation since no other suitable method of correction was found for the second order field, being better than no correction at all. Thus, the pole pieces have boundaries consisting of two circles with their centers at two different points.

5. Substitution of the Circular Magnetic Boundary for the Kerwin Field; Collimatron Arrangement

Kerwin, in his second paper published in 1949, illustrated how the ideal magnetic field could be divided on the plane $x=0$, which was probably possible from the fact that all incident ion beams in the Kerwin field tend to $dy/dx=0$ at $x=0$. If a field able to make a divergent beam parallel is available, a complete image system must be obtained by the combination of two such fields. Now the boundary of the Kerwin field can be reproduced as follows. When sliding an acute-angle vertex of a right-angle triangle along a line in such a way that the subtense of it will always pass one point not existing on the line, the locus of the right-angle vertex is the Kerwin field boundary, which can be drawn

mechanically but cannot be reproduced precisely with actual machining techniques. It would be convenient if we could devise ideal magnetic boundaries by a combination of straight lines or circles containing no other functional curves. Smythe[11] constructed a wide angle complete focusing mass spectrometer in 1934, in which the incident ion beam focuses on one point only when it is composed of parallel components. The shape of the magnetic field reported by Smythe is fringed by two circular boundaries so as to form a part of the crescent, and its mechanical shaping is possible, though not very easy. However, when the Smythe field is considered from the standpoint of dividing the ideal boundary, it offers the focusing half of the field, because the ideal field is divided at the plane, $x=0$, where the divergent ion beam is paralleled i.e., collimated. It is, therefore, clear that two sets of Smythe fields arranged in mirror symmetry with regard to the

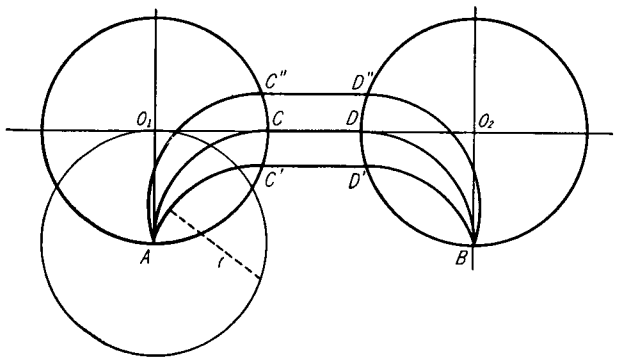

Fig. 10. New compound complete focusing field (Collimatron arrangement).

plane perpendicular to the direction of the incident parallel beam, where one half of the compound fields plays the role of the collimator, and the other the focaliser, which prepares the divided ideal boundary corresponding to the Kerwin field. The problem now is to find another optical system which will satisfy the wide angle focusing condition of the Smythe system, without the difficulties of machining as mentioned above. Now, a study of the treatment of the second order focusing of the $\pi/2$-field shows that for ion beams with a deflection radius as large as the radius of the field boundary, if they pass a fixed point on the incident boundary, then they leave the other boundary in parallel and at right angle to the central incident direction independently of that incident direction, and therefore, parallel beams which satisfy those conditions upon entering the field always pass the fixed point on the field boundary. This is nothing else than the theoretical complete focusing condition. Fig. 10 shows that the circular fields

when set face to face in this way give a complete focusing system as well as the divided Kerwin field. However, not only in this compound circular magnetic field, but also in the compound Smythe field, in contrast to the divided Kerwin field, the image character only remains, and the dividing plane of the linear boundary does not exist. Therefore, it is impossible to reduce these fields to a single field by joining the dividing planes as in the Kerwin field. While there have been various studies concerning a compound field, a geometrical-optical system where one field is, as it were, a collimator to make the beams parallel and the other field is used to focus the paralleled beams in order to make wide angle complete focusing has not yet been proposed. This system, named "Collimatron," therefore, is different from any other focusing system, and, if conformally represented with the use of complex space, corresponds to the aberrationless lens system consisting of non-spherical convex lens. Now, omitting the mathematical treatment, because the positive meaning of it is not included in this paper, we describe only that there is a conformal-representational relation between a purely optical system and a dynamical representational system.

Fig. 10 shows that, when the point A in the first magnetic field boundary expressed by the circle O_1 is a point source, the point B in the second field expressed by the circle O_2 is a focusing point, and in this case theoretically the beams can be focused over $\pm\pi/2$ with regard to the central beam. Practical considerations indicate that the beam must be confined because the fringing field becomes more and more effective as the direction of the beam nears that of the tangential line at its departure point, but Nier's approximation or other compensations are more effective in this type of field than in the Smythe field, taking the shape of the field into account.

The beam entering the field from the other point (A', not shown in figure) than A focuses also at the point B' on the circle O_2 and $\widehat{AA'}=\widehat{BB'}$. This feature of this field system is not realized by the Kerwin field, which produces complete focusing with a point source, but does not yield an aberrationless representation with a source having an actual width as in this case. In Fig. 10, the width of the collector slit at the focusing point being D, and $|AA'|=d$, the theoretical resolving power of such an instrument is written as below,

$$M/\Delta M = r/(d+D)\,. \tag{85}$$

As discussed before, the first field is used only as the collimator, and hence the intensities of the first and second magnetic fields being H_1 and H_2, respectively, and the radii of the boundaries r_1 and r_2, respectively, the geometrical conditions, if $H_1r_1=H_2r_2$, are the same as before independently of the radii of the two circular

boundaries. The theoretical resolving power in this case is expressed by the equation,

$$M/\Delta M = r_1 r_2/(dr_2+Dr_1)\,, \tag{86}$$

and then, putting $D=md$, $r_2=nr_1$, we obtain the following form,

$$M/\Delta M = r_1/2d(2n/(n+m))\,. \tag{87}$$

When $d=D$, $r_1/2d$ is the ideal aberrationless maximum resolving power corresponding to the radius of deflection of the single focusing magnetic field, and therefore, the resolving power of this system is equal to $r/2d$, when $n=1$, $m=1$, and two times $r_1/2d$ when $n\to\infty$, which shows that this system, if $n>1$, gives a larger resolving power than the ideal one of the single focusing system.

In conslusion, an optical system like this makes possible a rather bright instrument and is especially effective as an electromagnetic mass separator, because the deflection radius of this system is less than that of the large single focusing instrument when using an equal amount of material. The resolving power of this system is clearly larger than that of the other system with aberration as follows,

$$M/\Delta M = r/\left\{D+r\psi(\theta,\ r/d)\right\} < r/(d+D)\,. \tag{88}$$

In a field with aberration, the contribution of $r\psi(\theta,\ r/d)$ increases relatively in comparison with $d+D$ with an increase in size of the instrument. In addition, the ion path becomes longer, and the space charge effect can no longer be neglected, which decreases the actual resolving power below that expected. Hence the employment of the Collimatron arrangement in the Smythe-type as well as in the circular boundary type instrument is favorable both in theory and in practice. The increase of the fringing effect with an increase in the number of magnetic boundaries can be avoided to some extent by use of a magnetic flux shutter with an iron core or some other suitable correction device.

6. Summaries

In the first-order focusing field:

(1) If the ion beam has divergence but no thickness, the image width is such that $S_{\pi/3}>S_{\pi/2}>S_{\pi}$ on the $+\theta$ side and $S_{\pi}>S_{\pi/2}>S_{\pi/3}$ on the $-\theta$ side.

(2) If the ion beam has both thickness and divergence, S_{π} increases exactly as the thickness of the ion beam, but $S_{\pi/2}$ and $S_{\pi/3}$ increase almost exactly as the thickness of the ion beam only when n is large, and the difference between them is little noticed. Thus, the π- field is found to be more favorable than any other field when the ion beam has thickness.

In the second-order focusing field:

(3) If the ion beam has divergence but no thickness, the image width is such that $S_{\pi/3} > S_{\pi/2}$ on both $+\theta$ and $-\theta$ sides, and is much less than that in the first-order focusing field. This shows that the second order focusing is very effective for wide angle focusing.

(4) If the ion beam has both thickness and divergence, the image widths in both fields are not very different; and consequently, the Kerwin field is ideal only for a line source, and the second order focusing has only a slight effectiveness on the convergence of an ion beam with actual thickness.

Generally,

(5) The dependency of the total image width on the ratio of the slit width to the deflection radius is discussed and some information for designing the ion source slit and the collector slit was obtained.

Finally,

(6) A new complete focusing field arrangement, deduced from consideration of the divided Kerwin field, is realised with two circular $\pi/2$-fields, and their features and applicability are described.

Acknowledgment

The magnet material for the new type pole pieces was offered by the Sumitomo Kinzoku Co., to whom the authors are deeply thankful. The assistance of T. Kanagawa in this work is also deeply appreciated.

Literatures Cited

1) W. Henneberg, Ann. d. Physik, **19**, 335 (1934).
2) R. Herzog, Z. f. Physik, **89**, 447 (1934).
3) J. Mattauch, ibid., **89**, 786 (1934).
4) H. Hintenberger, Z. Naturforsch., **3a**, 125, 669 (1948); Rev. Sci. Instrum., **20**, 748 (1949).
5) L. Kerwin, Rev. Sci. Instrum., **20**, 36, 381 (1949); **21**, 96 (1950).
6) G. P. Barnard; "Modern Mass Spectrometry", The Institute of Physics, London, p. 29–30, (1953).
7) A. O. Nier, Rev. Sci. Instrum., **11**, 212 (1940).
8) N. Kadota, S. Ishida and T. Kanagawa, Shitsuryo Bunseki (Mass Spectroscopy), **11**, 52 (1958).
9) N. D. Coggeshall, J. Appl. Phys., **18**, 855 (1947).
10) Y. Sugawara, Shitsuryo Bunseki (Mass Spectroscopy), **12**, 34 (1959).
11) W. R. Smythe, L. H. Rumbaugh and S. S. West, Phys. Rev., **45**, 724 (1934).